

# The optimization of optical fiber-based surface plasmon resonance sensor with $\text{Ti}_3\text{C}_2$ MXene material

H. AHMAD<sup>1,2,3,4,\*</sup>, M. J. M. MAKHFUZ<sup>1</sup>, N. YUSOFF<sup>1</sup>

<sup>1</sup>Photonics Research Centre, Universiti Malaya, 50603 Kuala Lumpur, Malaysia

<sup>2</sup>Department of Physics, Faculty of Science, Universiti Malaya, 50603 Kuala Lumpur, Malaysia

<sup>3</sup>Distinguished Visiting Professor, Universiti Kuala Lumpur British Malaysian Institute (UniKL BMI), Batu 8, Jln Sungai Pusu, 53100 Selangor, Malaysia

<sup>4</sup>Adjunct professor, Department of Physics, Faculty of Mathematics and Natural Sciences, Universitas Negeri Malang, Jalan Semarang 5, Malang, 65145, Indonesia

The fabrication and optimization of a surface plasmon resonance (SPR) based fiber optic sensor for glucose detection is reported in this work. The sensing probe was prepared using an arc-shaped single-mode fiber (SMF-28) coated with gold and then a layer of MXene, 2D material. The sensitivity performance of the sensor towards glucose analyte was investigated, first with gold-coated fiber SPR sensor and then with gold that was overlaid with  $\text{Ti}_3\text{C}_2$  MXene. Different glucose concentrations ranging from 0.09 M to 1.30 M were tested and the spectral response of the sensor probe towards different concentrations of glucose was analyzed. It was found that the gold-coated fiber SPR sensor yields a sensitivity of 29.60 nm/M, and 33.06 nm/M for the gold-MXene coated fiber SPR sensor. The proposed study's findings show that gold with an overlay of MXene layer has provided a better sensitivity in glucose sensing applications.

(Received March 6, 2023; accepted October 9, 2023)

**Keywords:** SPR sensor, MXene, 2D material, Fiber-based sensor, Arc-shaped fiber

## 1. Introduction

Based on the World Health Organization (WHO), up until now, about 422 million patients are living with diabetes, and each year, around 1.5 million deaths are caused by the prevalent disease [1]. The level of blood glucose characterizes this chronic metabolic disease. It can be categorized into two main types where one (Type 1) occurs when the body doesn't produce enough insulin by the pancreas, and the second (Type 2) is when the insulin produced is underutilized [2]. Over time, excess glucose in the body may induce hyperglycemia, leading to complications and severe damage such as kidney failure, heart attacks, blindness, stroke, etc. [3]. Therefore, glucose concentration detection is essential for personal monitoring and clinical diagnosis to relieve many adults' sufferings.

Various glucose sensors have been continuously developed and evolved in the past years. Among the methods, electrochemical, chemiluminescence, and colorimetry analysis are some of the methods widely studied. For instance, Wu et al. [4] successfully fabricated the glucose oxidase-nanoporous gold co-catalysis ( $\text{GO}_x/\text{NPG}/\text{GCE}$ ) bioelectrode for glucose sensing, having excellent sensitivity, selectivity, and stability. Then in 2019, Zhu et al. [5] developed an attractive chemiluminescence-based sensor using 2D metal-organic

frameworks (2DMOFs)-Co-TCPP(Fe). Nevertheless, these methods suffer from high expenses, tedious operations, and involve complex modification processes. Besides that, prism or glass chip surface plasmon resonance (SPR) probes are also widely used to measure glucose in a sample [6,7]. With high specificity and sensitivity advantages, the prism or glass chip SPR technique has been rapidly used as biosensors [8–11]. However, this sensor suffers from its bulky and quite costly drawbacks, which may be difficult to apply in remote sensing. Thus, optical fiber-based sensors are of interest for biomedical sensing applications due to their unique advantages of low cost, remote sensing ability, flexibility, immunity to electromagnetic interference, and small size [12,13].

Fiber-based SPR sensors possess the extra merit of wide detection bandwidth, high-temperature operation, and robustness, making sensing applications easier [14]. However, the current shortcoming is the sensitivity due to the light constraint in the core. This may result in low sensor sensitivity. Hence, sensitivity-enhanced material can be implemented to increase the device's sensitivity further and improve the sensing performance. Many materials have been recently explored to provide higher sensitivity and selectivity of different sensing devices [15]. Two-dimensional (2D) materials, specifically, have sparked the enormous interest of researchers, namely, graphene, black phosphorus, MXene, and others. A study

conducted by Li et al. [16] achieved an improvement in the sensitivity for glucose detection by employing graphene oxide (GO) and multi-wall carbon nanotubes (MWCNTs) embedded on top of the serial quadruple taper fiber (SQTF)-based LSPR sensor. In the same year, Kumar et al. [17] successfully improved the sensitivity of the p-cresol biosensor by combining gold nanoparticles (AuNPs) and copper oxide nanoflowers (CuO-NFs) on a tapered-in-tapered fiber (TiTF) structure. In the following year, graphene oxide and multiwalled carbon nanotubes (GO/MWCNTs) were also demonstrated, resulting in an improvement in sensitivity of the taper-in-taper with four tapered (TIT4T) localized SPR sensor for alanine aminotransferase (ALT) enzyme detection [18]. Among the series of 2D materials, MXene is a promising sensing material due to its unique characteristics and properties [19,20]. Its accordion-like structure gives a large area for external interactions, and its hydrophilic feature makes it easier for the materials to combine with other organic solvents and organisms [21]. Surface modifications can also tune the characteristics of MXene and thus promote the material's variability [22].

In this study, the optimization of the sensor in terms of the gold thicknesses and fiber losses was done to achieve the best performance of the SPR sensor. In addition, the optimized gold-coated fiber SPR sensor and gold-MXene-coated fiber SPR sensor were also fabricated. The transmission spectra with different concentrations of glucose samples were recorded, and the sensitivity performance of both sensing devices was analyzed. Further, the stability of the measurements was examined by taking the transmission spectrum with fixed glucose concentration for about 90 minutes with 30 minutes intervals.

## 2. Experimental method

The following sub-section discusses the preparation of the  $\text{Ti}_3\text{C}_2$  MXene sample; section 2.2 provides the preparation of glucose samples, and section 2.3 discusses the fabrication of arc-shaped fiber. Finally, the preparation of the arc-shaped fiber-based SPR sensor and the SPR sensor setup is given in sections 2.4 and 2.5, respectively.

### 2.1. Preparation of $\text{Ti}_3\text{C}_2$ MXene sample

To prepare the exfoliated  $\text{Ti}_3\text{C}_2$ , *in situ* HF was used as the etchant, and the procedure applied was adopted from [23] with few modifications. The fabrication process is depicted in Fig. 1. *In situ*, HF etchant was prepared by adding lithium fluoride (LiF, 12 M) powder to hydrochloric acid (HCL, 9 M). First, 0.8 g of LiF and 10 ml of HCL were mixed and stirred continuously. With constant stirring applied, 0.5 g of titanium aluminum carbide ( $\text{Ti}_3\text{AlC}_2$ , 98 wt%) powder was added gradually, and the stirring proceeded for 48 hours at room temperature. Next, as the etching process was completed, the mixture was washed a few times by centrifugation (3500 rpm, 5 minutes) to separate the supernatant and the sediment. The pH value of the supernatant was measured, and if it displayed acidic, the supernatant was decanted, and the residue was again mixed with 150 ml of deionized (DI) water. The solution was centrifuged, and the washing cycle was repeated a few times until pH 4-5 was achieved. The black slurry was then collected and redispersed in 50 ml of DI water to proceed with the delamination process. The solution was shaken manually for a few seconds, and centrifugation was applied to separate the etched and nonetched MXene. The final step was to filter the flakes synthesized by vacuum-assisted filtration, and the collected powder was dried in a vacuum for a few days.

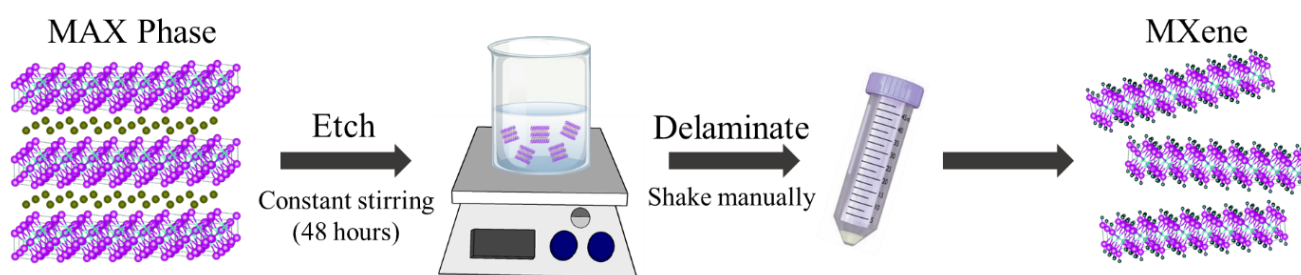


Fig. 1. Schematic diagram of the fabrication process of  $\text{Ti}_3\text{C}_2$  (color online)

### 2.2. Preparation of glucose samples

Different concentrations of glucose samples were prepared using the dilution equation,  $C_1V_1 = C_2V_2$ , where  $C_1$  and  $C_2$  represent the initial and desired concentrations, and  $V_1$  and  $V_2$  are the initial and final volumes, respectively [24]. First, the glucose was diluted in

deionized water to produce 0.09 M, 0.17 M, 0.26 M, 0.35 M, 0.43 M, 0.87 M, and 1.30 M concentrations. The samples were then sonicated for about 30 minutes to ensure the glucose powder was fully dissolved in the DI water solvent. Several different concentrations are needed to determine the effectiveness of the sensor in detecting glucose samples.

### 2.3. Fabrication of arc-shaped fiber

The arc-shaped fiber was prepared using the wheel polishing technique with the setup, as shown in Fig. 2. A standard single-mode fiber (SMF-28) with a core and cladding diameters of 9  $\mu\text{m}$  and 125  $\mu\text{m}$ , respectively, was used. First, about 3 cm of the fiber was stripped and cleaned with alcohol. Then, the surface of the stripped fiber was suspended onto the mechanical wheel with a 2 cm diameter, wrapped with abrasive sandpaper. Next, the

fiber was clamped to ensure it was fixed. A laser light source was connected at one end of the fiber, and the other was connected to the optical power meter to monitor the loss of the fiber. The fiber was then polished until a loss of 2.0 dB was achieved, and then the arc-shaped fiber was fixed onto a glass slide to handle the as-prepared fiber during the sensing process. The polishing procedure was repeated to get different arc-shaped fibers with 2.3 dB, 2.5 dB, and 2.7 dB losses.

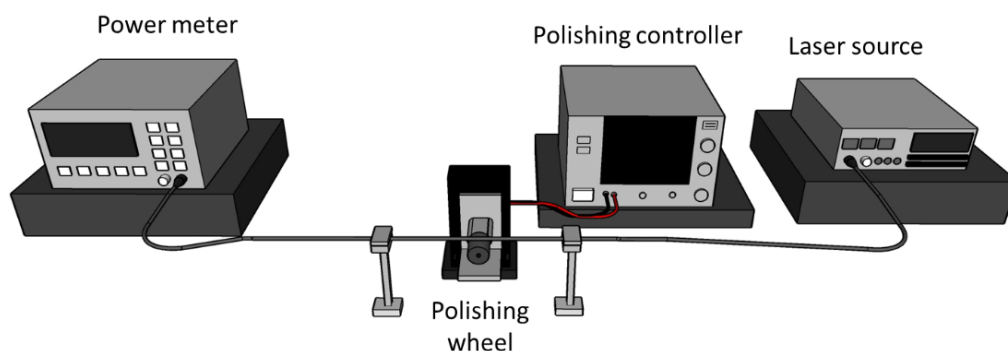


Fig. 2. Arc-shaped fiber preparation setup

### 2.4. Preparation of arc-shaped fiber-based SPR sensor

The fabricated arc-shaped fiber was first treated and cleaned with piranha solution ( $\text{H}_2\text{SO}_4 + 30\% \text{H}_2\text{O}_2$ , 7:3) to remove any trace of organic residues on the fiber surface. The fiber was then rinsed a few times with deionized water and was let dry in an open space for a few hours. Next, the treated, polished surface was coated with a gold layer using an electron beam deposition technique. The chamber's pressure was set at  $10^{-5}$  to  $10^{-7}$  Torr. In the chamber, the current supplied flows through the tungsten filament and emits electrons causing them to hit the targeted metal. The atoms from the gold metal will then transform into the gaseous phase and precipitate into solid form to uniformly coat the fiber sample in the chamber. Different layer thicknesses, such as 40 nm, 50 nm, and 60 nm of gold, were deposited onto the as-prepared fibers to study the effect of these gold thicknesses on the SPR signal. After that, to prepare the gold overlaid MXene SPR sensor, the gold-coated arc-shaped fiber was again treated with piranha solution to hydroxylate the surface of the sensing probe. Then, the sample was dip-coated with  $\text{Ti}_3\text{C}_2$  MXene solution (15 mg/ml) for about 2 hours to allow the immobilization of the MXene onto the sensing surface. Finally, the fiber was dried in the open air before being introduced in the sensing setup. The schematic illustration of the gold-MXene coated fiber SPR configuration is shown in Fig. 3, where the polished surface was covered with gold and  $\text{Ti}_3\text{C}_2$  MXene.

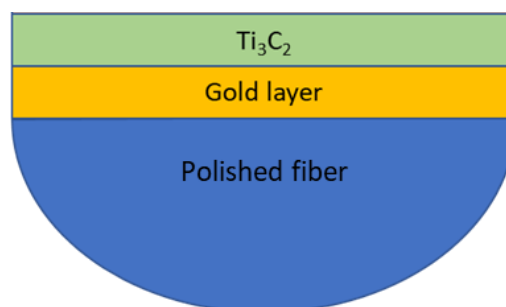


Fig. 3. Schematic diagram of the prepared gold-MXene coated fiber SPR configuration (color online)

### 2.5. Fiber-based SPR sensor setup

The experimental setup used to detect glucose is shown in Fig. 4. The sensor's input was coupled to a white light source, and the output was analyzed using an Ocean Optic spectrometer connected to a computer with OceanView software. By applying different concentrations of glucose analyte ranging from 0.09 M to 1.30 M, the changes in the output transmission spectrum were observed and recorded. DI water was used to simulate the SPR spectrum under different thicknesses of gold and fiber losses to find the optimal gold film and fiber cladding thickness. The first experiment was carried out to analyze the SPR transmission of various losses of arc-shaped fiber with the same thickness of the gold layer. Then, the SPR effect of the arc-shaped fiber sensor with different thicknesses of the gold layer was also studied. Lastly, the sensitivity of the as-prepared gold-coated fiber SPR sensor and gold-MXene-coated fiber SPR sensor towards different glucose concentrations were also analyzed.

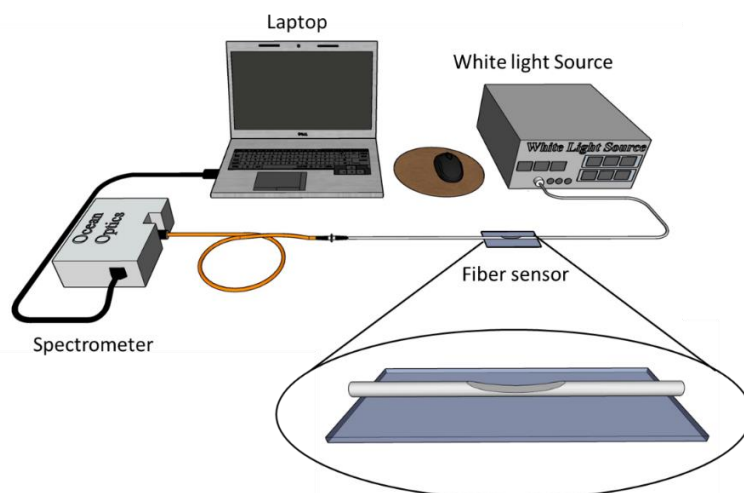


Fig. 4. Fiber optic SPR experimental setup

### 3. Results and discussion

#### 3.1. Characterization of $\text{Ti}_3\text{C}_2$

##### 3.1.1. High-resolution transmission electron microscopy (HRTEM)

The morphological structure of the as-synthesized MXene was characterized by HRTEM, as displayed in Fig.

5. Fig. 5(a) shows the 2D nanosheet characteristics found in the sample. The layers are pretty thin, and it can be seen that there are some formations of a single layer or multiple layers stacked on one another. Fig. 5(b) shows the cross sections of the multi-layered  $\text{Ti}_3\text{C}_2$  nanosheets, and the interlayer spacing measured was about 1.04 nm.

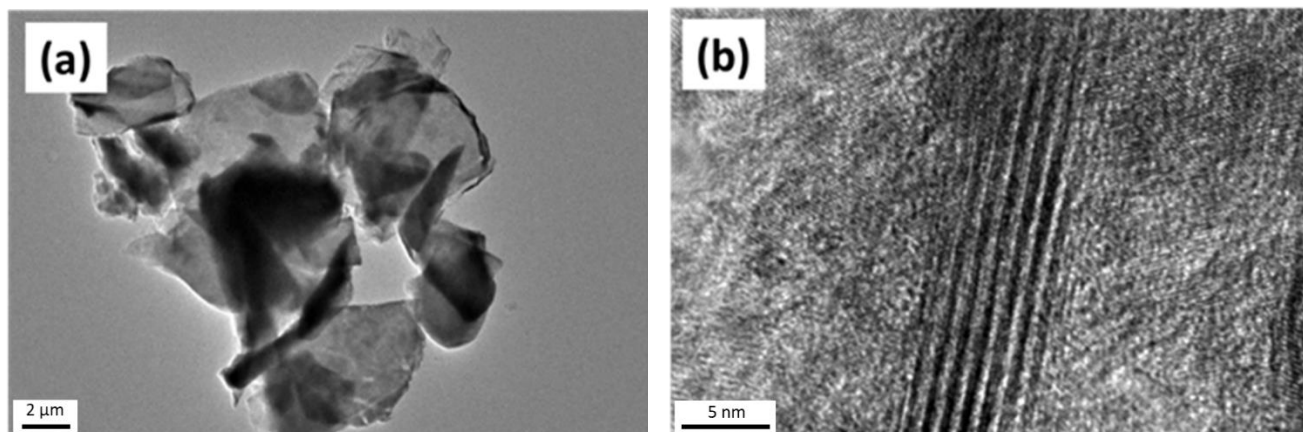


Fig. 5. HRTEM images of  $\text{Ti}_3\text{C}_2$  with (a) low magnification and (b) high magnification

##### 3.1.2. Field Emission Scanning Electron Microscope (FESEM) & Energy Dispersive X-Ray Analysis (EDX)

The FESEM image of  $\text{Ti}_3\text{C}_2$  MXene is displayed in Fig. 6(a). It shows clear multi-layered nanosheet morphology, which also resembles exfoliated graphite. It is evident in the sample that a large number of 2D flakes can be seen scattered and stacked onto one another, and an apparent lamellar structure can be observed, as in Fig. 6(a). EDX analysis was also done, where the elemental mapping of  $\text{Ti}_3\text{C}_2$  and the elemental composition present

in the as-synthesized sample is shown in Fig. 6(b). The elemental analysis results can be summarized in Table 1. It can be seen that the aluminum (Al) elements that exist in the sample are almost depleted, which shows the success of the etching process. The titanium (Ti) and carbon (C) elements are the main elements in the prepared  $\text{Ti}_3\text{C}_2$  MXene.

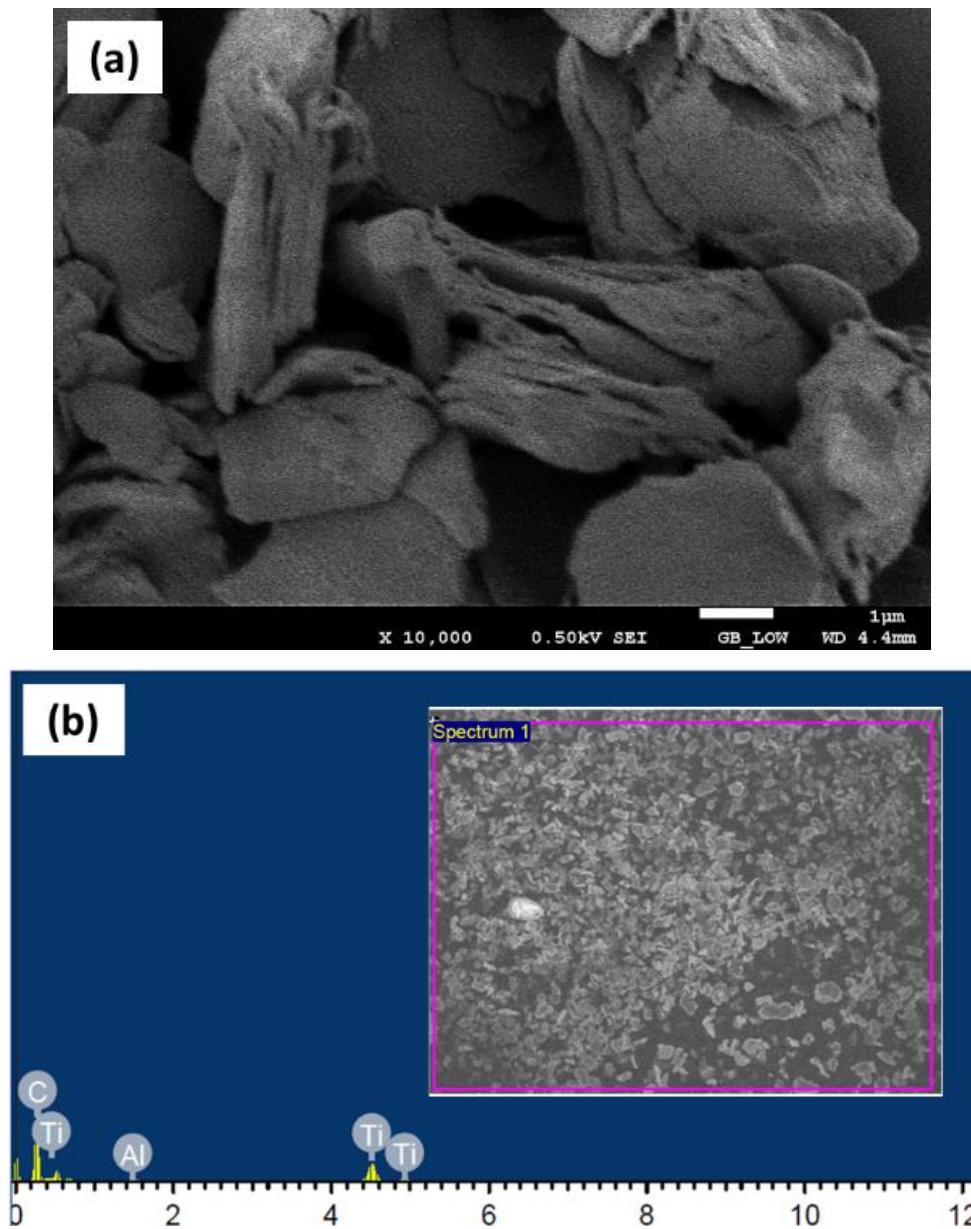


Fig. 6. (a) FESEM image of  $Ti_3C_2$ , (b) EDX analysis and the spatial distributions of  $Ti_3C_2$  (color online)

Table 1. EDX analysis results for  $Ti_3C_2$  sample

Elements	Atomic No.	Weight [%]	Atomic [%]
Titanium (Ti)	22	30.47	9.93
Carbon (C)	6	69.11	89.83
Aluminum (Al)	13	0.41	0.24

### 3.1.3. Ultraviolet (UV)/visible (Vis)/near-infrared (NIR)

Fig. 7 shows the ultra-violet and visible (UV-Vis)/near-infrared (NIR) spectroscopy results of  $Ti_3C_2$  MXene. It can be seen that it exhibits a broad UV absorption spectrum from 200 - 1300 nm wavelength. A prominent peak is evident at a wavelength of about 230 nm, which corresponds to the band-gap energy of the oxidized MXene, as mentioned by [25].

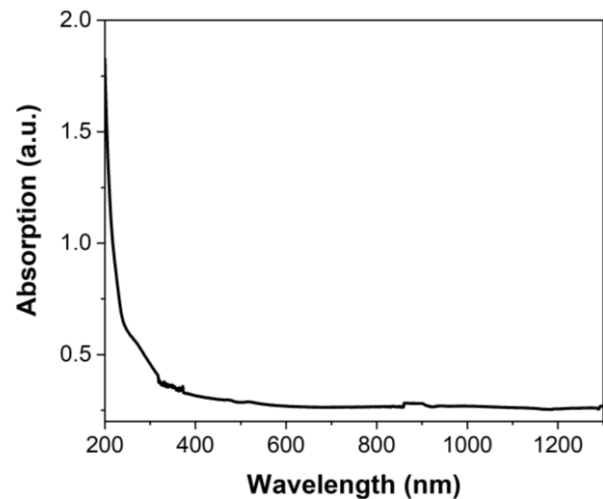


Fig. 7. UV-Vis NIR analysis of  $Ti_3C_2$

### 3.2. Surface plasmon resonance fiber-based sensor

The working principle of the fiber-based SPR sensor [26] is the same as the traditional prism SPR technique, and the schematic diagram is shown in Fig. 8(a). First, the light is generally transmitted from one end to another by total internal reflection in the fiber's core. Then, the guided light may result in the formation of the evanescent wave at the core-cladding interface. The propagations of the

evanescent wave along the core-cladding interface will then excite the surface plasmons at the metal-sensing layer interface. The excitation of surface plasmons occurs as the energy from incident light is transferred to the surface plasmons at the metal/dielectric interface and, thus, reduces the transmitted light intensity. A sharp dip can be observed from the transmission spectrum, as shown in Fig. 8(b), at a particular wavelength (nm) due to the efficient energy transfer.

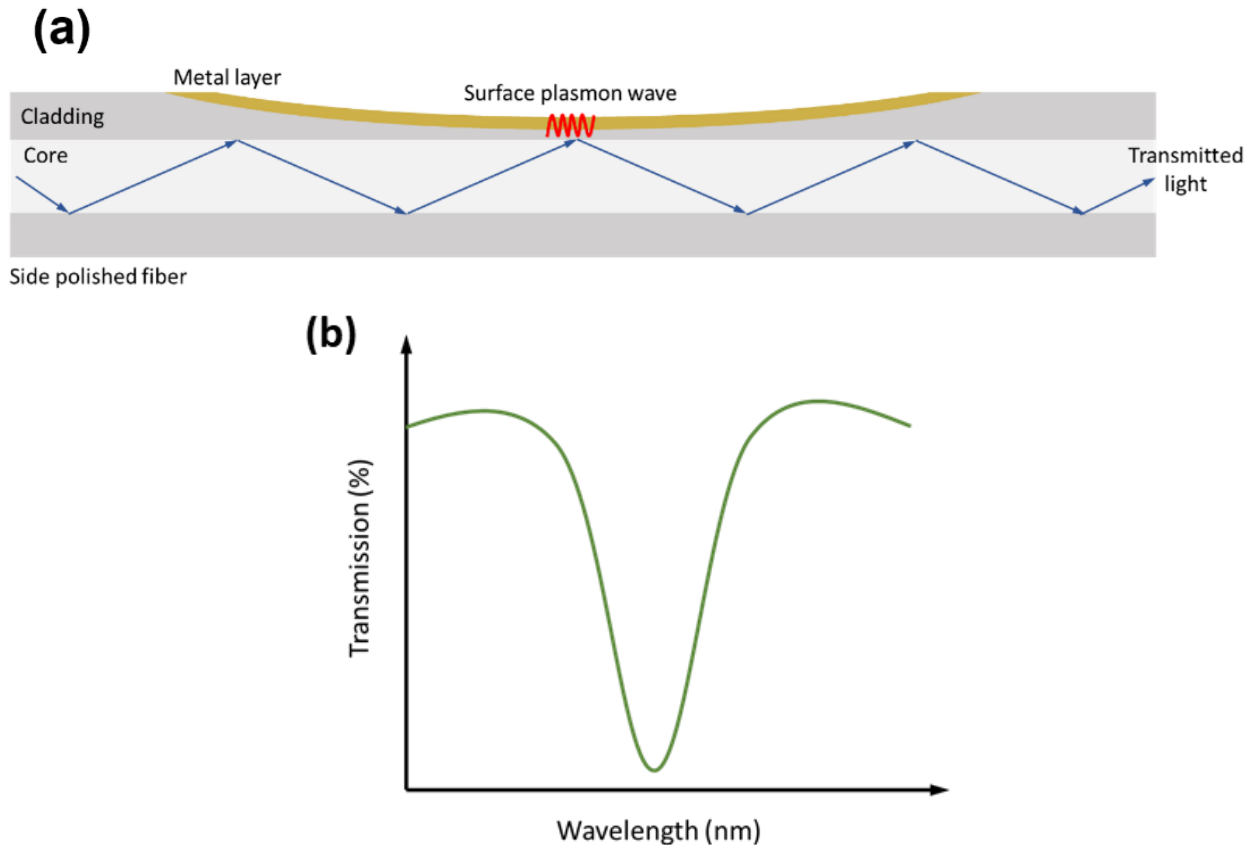


Fig. 8. Schematic representation of (a) fiber-based SPR sensing principle and (b) SPR spectrum

#### 3.2.1. Various arc-shaped fiber losses

An excellent SPR sensor having high sensitivity can be assessed by investigating the SPR curve depth. An analysis called the full width at half maximum (FWHM) analysis was carried out to study the sensing capability of the SPR sensor. It was obtained by determining the width of the SPR curve at half of its maximum intensity. Specifically, the maximum loss of the transmitted power was first measured, and half of its maximum was calculated. The difference of the wavelengths corresponding to the half maximum points was calculated to obtain the FWHM value [27]. A sharper and narrow resonance dip will result in a smaller value of FWHM, enhancing the sensing capability and improving the sensor resolution. The prepared device was first connected to the light source and a spectrometer, as mentioned in the SPR

setup. Fig. 9(a) displays the resonance dip when tested with DI water with different losses of arc-shaped fiber applied with a fixed gold film thickness of 50 nm. The fiber was polished with 2.0 dB, 2.3 dB, 2.5 dB, and 2.7 dB losses, and taking into account the FWHM of each SPR spectrum, arc-shaped fiber coated with a gold layer having 2.3 dB loss has the narrowest resonance dip of about 87.64 nm. To achieve a high-sensitivity sensor, a 2.3 dB loss of arc-shaped fiber was chosen as the sensing probe for the experiment as it gives the optimal cladding depth for the evanescent wave interaction. The microscopic image of the prepared arc-shaped fiber (2.3 dB) is shown in Fig. 9(b), where the diameter and length of the device obtained were about 67.6  $\mu\text{m}$  and 2.2 mm, respectively. Fig. 9(c) shows the cross-section of the arc-shaped fiber, (i) before and (ii) after 2.3 dB loss was achieved from the polishing process.

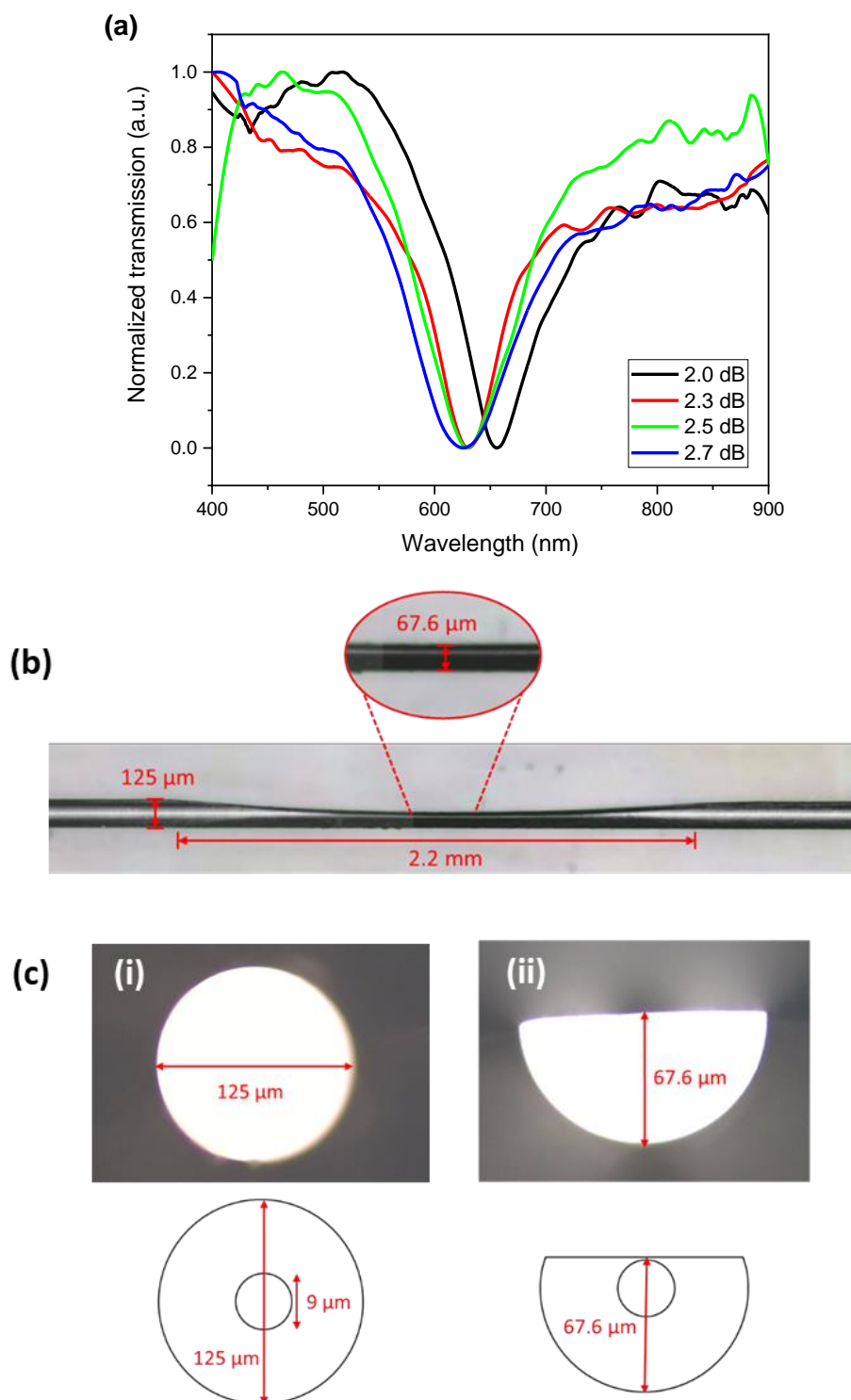


Fig. 9. (a) Transmission spectra for gold-coated arc-shaped fiber with different insertion losses, (b) microscopic image of arc-shaped fiber (2.3 dB), (c) cross-sectional view of (i) stripped SMF-28 and (ii) polished SMF-28 (2.3 dB) (color online)

### 3.2.2. Various Au layer thicknesses SPR analysis

Fig. 10 shows the transmission spectra of the sensor with different thicknesses of gold layer (40 nm, 50 nm, and 60 nm) coated on the arc-shaped fiber. The insertion loss of the polished fibers was fixed at about 2.3 dB. From the spectra in Fig. 10, different transmitted resonance dips

can be observed, and the FWHM values for 40 nm, 50 nm, and 60 nm gold layers were measured to be 105.1 nm, 87.7 nm, and 95.0 nm, respectively. The narrowest FWHM obtained was when the gold film thickness was about 50 nm. Thus, a 50 nm thickness of the gold layer was chosen explicitly for a further experiment as it gives a better sensitivity [28,29] than the 40 and 60 nm of gold coating.

Thus, a 2.3 dB loss of arc-shaped fiber coated with 50 nm gold film was used as the optimal conditions for the sensing device.

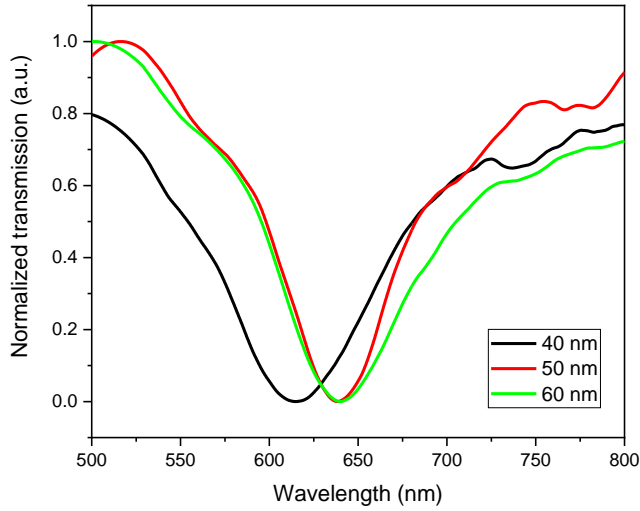


Fig. 10. SPR transmission with different thicknesses of the gold layer (color online)

### 3.2.3. Various glucose tests using the gold-coated fiber SPR sensor

After the SPR fiber sensor optimization, DI water and different glucose concentrations ranging from 0.09 M to 1.30 M were tested, and the SPR spectra are shown in Fig. 11. It can be observed that the fiber coated with a 50 nm thickness of gold film to generate the SPR signal has quite low sensitivity, where only a slight shift in resonance dip was detected as the concentration of glucose changed. From the graph, the SPR wavelength has a redshift from 643.08 nm to 662.67 nm as glucose concentration increased from 0 M to 1.30 M.

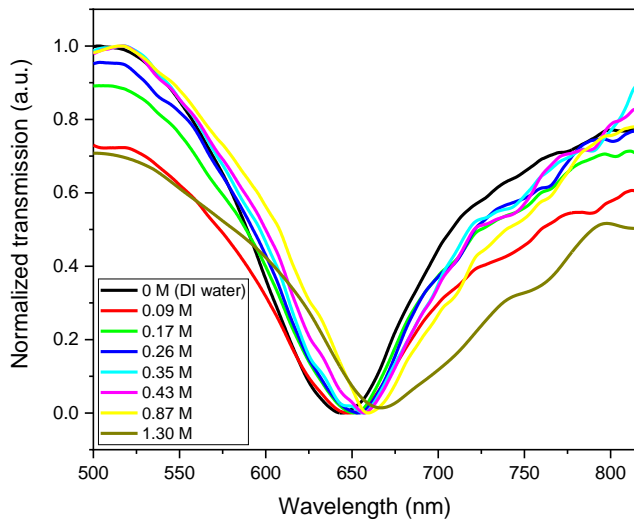


Fig. 11. SPR transmission when different glucose concentrations are tested using the gold-coated fiber SPR sensor (color online)

### 3.2.4. Various Glucose tests using the gold-MXene coated fiber SPR sensor

The sensitivity of the sensing device can be tailored by coating the as-prepared SPR sensing surface with a gold layer and overlay with a 2D MXene material, Ti<sub>3</sub>C<sub>2</sub>. The device was again tested with different concentrations of glucose solution, and the spectra are shown in Fig. 12. A noticeable wavelength shift can be observed compared to the gold-coated fiber optic SPR sensor. The resonance wavelength redshifts towards a longer wavelength from 638.44 nm to 682.56 nm as the concentration changed from 0 M to 1.30 M. The shifts in resonance dip measured were around 19.59 nm for the gold-coated fiber SPR sensor and 44.12 nm for the gold-MXene-coated fiber SPR sensor. Therefore, it can be concluded that this configuration of the SPR sensor contributes to a higher shift than the gold-coated fiber SPR sensor.

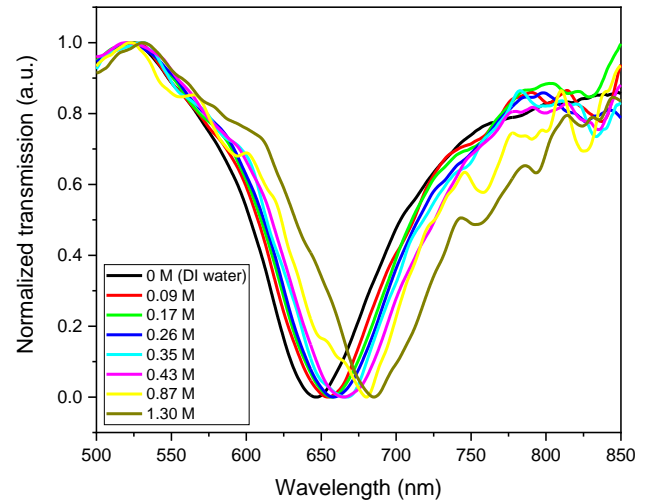


Fig. 12. SPR transmission of different glucose concentrations using gold-MXene coated fiber SPR sensor (color online)

### 3.2.5. Fiber-based SPR sensor sensitivity analysis

In this research, the sensitivity of a sensor can be defined by the change in the resonance wavelength for a unit change in the concentration of the analyte. Generally, the sensitivity can be obtained by eq. (1):

$$S_n = \frac{\delta\lambda}{\delta C} \quad (1)$$

where  $\delta\lambda$  is the resonance wavelength change, and  $\delta C$  is the concentration change [30]. A linear regression graph of resonance wavelength change versus concentration change can be plotted, and the sensitivity can be obtained from the slope of the linear regression fitting line [31]. The sensitivity of both sensors towards different concentrations of glucose with molecular formula C<sub>6</sub>H<sub>12</sub>O<sub>6</sub> was determined. Fig. 13 depicts the linear regression graph, along with the sensitivity equation and the regression coefficient R<sup>2</sup> value for each of the sensors. The plotted data for the gold-coated fiber SPR sensor was separated

into two distinct regions. This indicates the sensor has two different functions, each covering a specific range of glucose concentrations. The first region corresponds to the concentrations ranging from 0 to 0.4 M, while the second part covers the concentrations from 0.4 M to 1.4 M. From the graph, it is also apparent that the gold-MXene coated fiber SPR sensor is capable of covering a much wider linear concentration range than that of the gold-coated fiber SPR sensor. The relationship between the SPR wavelength shift and glucose concentrations for the gold-coated fiber SPR sensor in the first region can be given by the equation  $\Delta\lambda$  (nm) = 29.60 [C<sub>6</sub>H<sub>12</sub>O<sub>6</sub>] + 2.01 and  $\Delta\lambda$  (nm) = 6.98 [C<sub>6</sub>H<sub>12</sub>O<sub>6</sub>] + 10.29 for the second region, with R<sup>2</sup> value of 0.962 and 0.992, respectively. Whereas the gold-MXene coated fiber SPR sensor has the relationship of Eq.,  $\Delta\lambda$  (nm) = 33.06 [C<sub>6</sub>H<sub>12</sub>O<sub>6</sub>] - 0.50 with an R<sup>2</sup> of 0.992. The gradient of the plotted graph defines the sensor's sensitivity. From the linear regression analysis, the gold-coated fiber SPR sensor yielded a gradient of 29.60 nm/M in the first and 6.98 nm/M in the second regions, and a higher sensitivity of about 33.06 nm/M was obtained for the gold-MXene coated fiber SPR sensor. The standard deviation value of 5 data sets was also calculated and presented as an error bar, as shown in the linear regression graph.

From the same graph, the limit of detection (LOD) can also be calculated using the estimation method proposed by the International Union of Pure and Applied Chemistry (IUPAC) [32,33] through the standard deviation of the response of the curve and the slope of the linear regression following the equation as follows:

$$LOD = \frac{3\sigma_y}{m} \quad (2)$$

where  $\sigma_y$  represents the standard deviation of the y-intercepts of the regression line, m is the slope of the linear regression line obtained from the calibration curve,

and the value 3 signifies the numerical factor that depends on the confidence level [34]. For the gold-coated fiber SPR sensor, the LOD was calculated by focusing on the first linear segment. With  $m$  and  $\sigma_y$  of 29.60 nm/M and 1.11 nm, the LOD of the sensor was calculated to be 0.11 M. While for the gold-MXene coated fiber SPR sensor, with  $m$  of 33.06 nm/M and  $\sigma_y$  of 0.72 nm, the LOD has a value of 0.07 M.

Table 2 shows the comparison of the performance of different optical fiber sensors for glucose analyte detection. Comparing the sensitivity, the arc-shaped/MXene-based fiber SPR sensor exhibits the highest sensitivity value, which is approximately 8 times better than the study conducted by Zhong et al. [35] and Kumeria et al. [36]. Zhong et al. utilized a helical intermediate-period fiber grating (HIPFG) sensor, while Kumeria et al. employed nanoporous anodic alumina rugate filters (NAA-RFs) sensor for glucose detection. Long-period fiber grating was also demonstrated in glucose sensing, where Chang et al. [37] used a notched long-period fiber grating (NLPGF) sensor, while Kim et al. [38] used a simpler version of only a long-period fiber grating (LPFG) sensor for glucose concentration measurements with a sensitivity of 0.147 nm/wt% and 0.0031 nm/wt%, respectively. Cho et al. [39] also conducted a study on optical fiber glucose sensing using a polymer microdisk photonic sensor integrated into silicon, with a sensitivity of 0.12 nm/wt%. The gold-MXene coated fiber SPR sensor used in this study exhibited a remarkably high sensitivity compared to other works. This is attributed to the active layer MXene on the Au surface, which played a crucial role in glucose detection, resulting in a positive relationship between various glucose concentrations and wavelength shifts. As for the LOD, a much lower LOD value was obtained by Zhong et al. and Kumeria et al. but the sensitivity obtained in this study indicates that the fabricated sensor holds excellent potential for glucose analyte detection.

Table 2. Comparison of different fiber-based optical sensors for glucose detection

Type of sensor	Sensitivity	Limit of detection (LOD)	Ref.
Arc-shaped/MXene-based fiber SPR sensor	33.06 nm/M 2.876 nm/wt%	0.07 M 0.70 wt%	This work
Helical intermediate-period fiber grating (HIPFG) sensor	4.643 nm/M	0.005 M	[35]
Nanoporous anodic alumina rugate filters (NAA-RFs) sensor	4.93 nm/M	0.01 M	[36]
Notched long-period fiber grating (NLPGF) sensor	0.147 nm/wt%	N/A	[37]
Long-period fiber grating (LPFG) sensor	0.0031 nm/wt%	N/A	[38]
Polymer microdisk photonic sensor	0.12 nm/wt%	N/A	[39]

2D materials interact well with biomolecules, and adding a  $\text{Ti}_3\text{C}_2$  layer on the fabricated fiber sensor has rapidly enhanced the sensitivity due to their strong interactions with one another [40,41]. The unique properties of hydrophilic surfaces, the high binding energy of biomolecules, and the chemical and mechanical stability of MXene also improve the SPR sensing performance [42]. In addition,  $\text{Ti}_3\text{C}_2$  MXene has a large surface area and high loading capacity, providing a broad platform for the binding and absorption of glucose molecules. The high surface-to-volume ratio allows an abundant functional group to attach to its surface and thus plays a crucial role in its chemical reactivity. The use of LiF in synthesizing

the *in situ* HF etchant enables the production of hydroxyl ( $-\text{OH}$ ) and fluorine ( $-\text{F}$ ) functional groups. The  $-\text{F}$  and  $-\text{OH}$  functionalized surface creates active sites that interact with multiple  $-\text{OH}$  functional groups contained in the glucose's structure through hydrogen bonding [43,44]. The hydrogen bond facilitates the selective and specific binding of glucose molecules to the MXene surface, making  $\text{Ti}_3\text{C}_2$  suitable for use as a sensing material to enhance sensor capabilities. Thus, based on the experimental work, it shows that the arc-shaped gold-coated fiber SPR sensor with the addition of  $\text{Ti}_3\text{C}_2$  MXene layer on the sensing surface increases the sensitivity of the sensor.

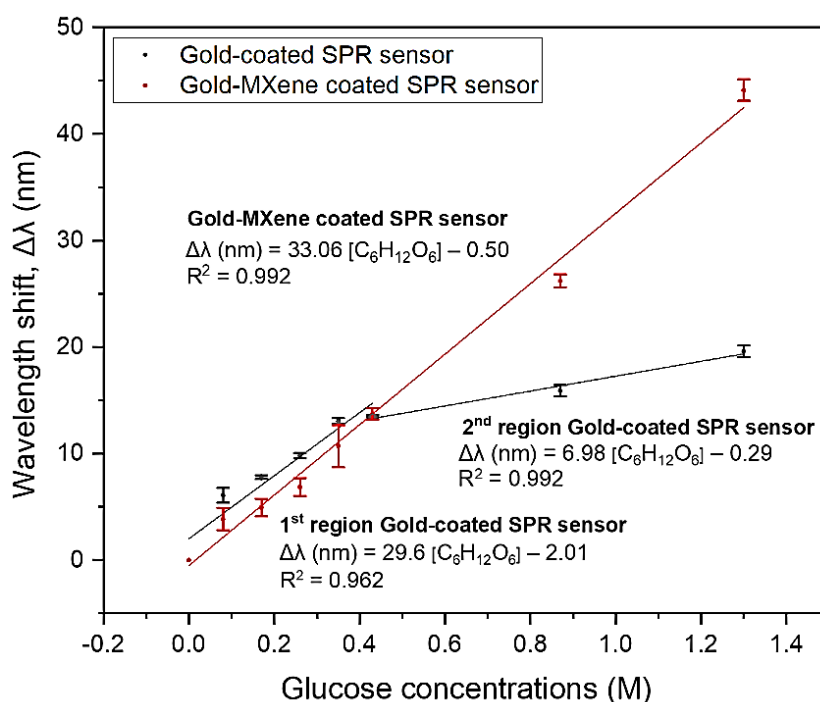


Fig. 13. Sensitivity analysis with change in glucose concentrations (color online)

### 3.2.6. SPR fiber-based sensor stability analysis

In addition, the stability of the sensor was also examined at a fixed 0.87 M glucose concentration for 90 minutes. The resonance dip wavelength for every 30-minute interval was recorded, and the wavelength evolution is shown in Fig. 14. It is very stable over the testing period. The resonance dip was maintained at a wavelength of around 676 nm throughout the stability measurement, and no distortion or inconsistency of wavelength shift can be observed from the analysis. The calculated standard deviation (STD) value was 1.801, where the low STD value indicates that the sensor possessed high stability even after a long period.

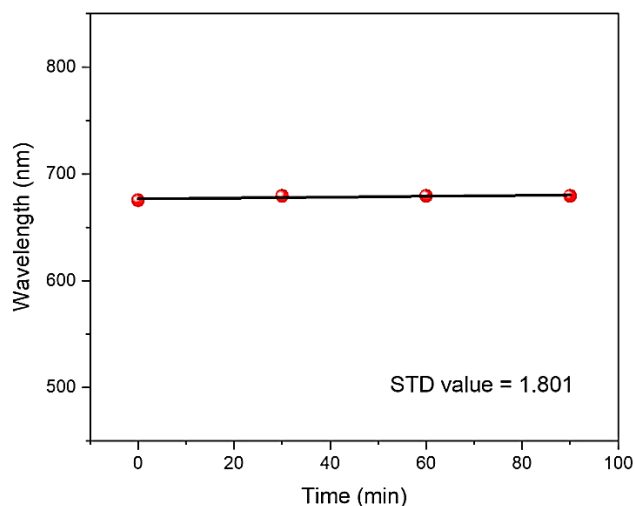


Fig. 14. The shift of wavelength against time

#### 4. Conclusions & Outlooks

In summary, the optimization of the SPR sensor in terms of the gold thicknesses and fiber losses was studied. The sensing device was prepared by polishing a single-mode fiber using the polishing wheel technique. A gold layer film was coated using the e-beam coating method to get a homogenous metal layer coating. As for the MXene, the layer was coated using the dip coating technique. It was found that a 2.3 dB loss of arc-shaped fiber coated with 50 nm gold film was the optimal condition to be used for the sensing device. For the gold-coated fiber SPR sensor, 29.60 nm/M sensitivity was measured with a LOD of about 0.11 M. The gold-MXene sensor's sensitivity was enhanced to a value of 33.06 nm/M with a LOD of 0.07 M. According to the results obtained, there is no doubt that the  $Ti_3C_2$  MXene will have extensive application and development in the future. The advantage of MXene is due to its unique characteristics and properties, making it suitable for fiber optic SPR sensors. The biocompatibility, low cost, remote sensing, small quantity, and low power consumption are some of the advantages owned by the proposed glucose sensor, which will have good potential for various applications in many fields, especially in biomedical sciences. The rapid enhancement of the SPR fiber-based glucose sensor's performance made the material prominent for promising applications in SPR biosensors. However, further improvements need to be made to improve the efficiency and overall effectiveness of the sensing device. In this experimental work, the gold-MXene coated fiber SPR device still has some drawbacks in controlling the uniformity and thickness of the  $Ti_3C_2$  layer. This may affect the consistency and reproducibility of the sensor. Thus, the method of accurately and uniformly controlling the MXene layer on the surface of the fiber optic sensor needs to be studied in depth to improve the reliability of the sensing device. As for future outlooks, more efforts should be given to the coating process of the  $Ti_3C_2$  2D material to achieve a homogenous and uniform  $Ti_3C_2$  layer. Also, a detailed study needs to be conducted on the surface chemistry of the  $Ti_3C_2$  MXene and its optical properties in relation to SPR. This will enable improvements and optimizations of the sensing device, ultimately increasing the detection accuracy even at a lower concentration range.

#### Declaration of competing interest

The authors declare that they have no known competing financial interests or personal relationships that could have appeared to influence the work reported in this paper.

#### Acknowledgment

This work was supported by the Ministry of Higher Education for the Fundamental Research Grant Scheme

(FRGS/1/2021/STG07/UM/01/1) and the HICOE grant (PRC-2022). This work was also partially funded by Universiti Malaya (RU005-2021).

#### References

- [1] D. M. Nathan, S. Genuth, J. Lachin, P. Cleary, O. Crofford, M. Davis, L. Rand C. Siebert, N. Engl. J. Med. **329**(14), 977 (1993).
- [2] P. Z. Zimmet, D. J. Magliano, W. H. Herman, J. E. Shaw, Lancet Diabetes Endocrinol. **2**(1), 56 (2014).
- [3] R. H. Eckel, W. W. Barouch, A. G. Ershow, Circulation **105**(24), 2923 (2022).
- [4] C. Wu, H. Sun, Y. Li, X. Liu, X. Du, X. Wang, P. Xu, Biosens. Bioelectron. **66**, 350 (2015).
- [5] N. Zhu, L. Gu, J. Wang, X. Li, G. Liang, J. Zhou, Z. Zhang, J. Phys. Chem. C **123**(14), 9388 (2019).
- [6] W. W. Lam, L. H. Chu, C. L. Wong, Y. T. Zhang, Sens. Actuators B Chem. **105**(2), 138 (2005).
- [7] Q. H. Phan, Y. R. Lai, W. Z. Xiao, C. H. Lien, Opt. Express **28**(17), 24889 (2020).
- [8] P. S. Pandey, S. K. Raghuvanshi, A. Shadab, M. T. I. Ansari, U. K. Tiwari, S. Kumar, IEEE Sens. J. **22**, 13800 (2022).
- [9] N. A. S. Omar, Y. W. Fen, J. Abdullah, Y. M. Kamil, W. M. E. M. M. Daniyal, A. R. Sadrolhosseini, M. A. Mahdi, Sci. Rep. **10**(1), 2374 (2020).
- [10] F. B. K. Eddin, Y. W. Fen, N. A. S. Omar, J. Y. C. Liew, W. M. E. M. M. Daniyal, Spectrochim. Acta Part A Mol. Biomol. Spectrosc. **263**, 120202 (2021).
- [11] F. C. Dudak, İ. H. Boyacı, Biotechnol. J. Healthc. Nutr. Technol. **4**(7), 1003 (2009).
- [12] S. Kumar, N. Agrawal, C. Saha, R. Jha, Optical Fiber-based Plasmonic Biosensors: Trends, Techniques, and Applications, ISBN 9781032152370, CRC Press (2022).
- [13] Y. Wang, Y. Huang, H. Bai, G. Wang, X. Hu, S. Kumar, R. Min, Biosensors **11**(12), 472 (2021).
- [14] Z. Wang, W. Zhang, X. Liu, M. Li, X. Lang, R. Singh, C. Marques, B. Zhang, S. Kumar, Biosensors **12**(11), 1016 (2022).
- [15] M. Li, R. Singh, Y. Wang, C. Marques, B. Zhang, S. Kumar, Biosensors **12**(10), 843 (2022).
- [16] G. Li, Q. Xu, R. Singh, W. Zhang, C. Marques, Y. Xie, B. Zhang, S. Kumar, IEEE Sens. J. **22**(17), 16904 (2022).
- [17] S. Kumar, Y. Wang, M. Li, Q. Wang, S. Malathi, C. Marque, R. Singh, B. Zhang, IEEE Sens. J. **22**(19), 18493 (2022).
- [18] R. Singh, Z. Wang, C. Marques, R. Min, B. Zhang, S. Kumar, Bioelectron. **236**, 115424 (2023).
- [19] A. Sinha, H. Zhao, Y. Huang, X. Lu, J. Chen, R. Jain, Trends Anal. Chem. **105**, 424 (2018).
- [20] H. Riazi, G. Taghizadeh, M. Soroush, ACS Omega **6**(17), 11103 (2021).
- [21] J. A. Kumar, P. Prakash, T. Krithiga, D. J. Amarnath, J. Premkumar, N. Rajamohan, M. Rajasimman, Chemosphere **286**, 131607 (2022).
- [22] J. Yoon, M. Shin, J. Lim, J. Y. Lee, J. W. Choi,

- Biosensors **10**(11), 185 (2020).
- [23] M. Alhabeb, K. Maleski, B. Anasori, P. Lelyukh, L. Clark, S. Sin, Y. Gogotsi, *Chem. Mater.* **29**(18), 7633 (2017).
- [24] W. M. E. M. M. Daniyal, Y. W. Fen, J. Abdullah, A. R. Sadrolhosseini, S. Saleviter N. A. S. Omar, *Spectrochim. Acta - Part A Mol. Biomol. Spectrosc.* **212**, 25 (2019).
- [25] E. Satheeshkumar, T. Makaryan, A. Melikyan, H. Minassian, Y. Gogotsi, M. Yoshimura, *Sci. Rep.* **6**(1), 32049 (2016).
- [26] B. D. Gupta, R. K. Verma, *J. Sensors* **2009**, Article ID 979761 (2009).
- [27] A. K. Paul, *OSA Continuum* **3**(8), 2253 (2020).
- [28] C. Teng, S. Ying, R. Min, S. Deng, H. Deng, M. Chen, X. Chu, L. Yuan, Y. Cheng M. Xue, *Sensors* **22**(16), 6241 (2022).
- [29] L. Liu, Z. Liu, Y. Zhang, S. Liu, *IEEE Sens. J.* **21**(15), 16621 (2021).
- [30] B. D. Gupta, R. Verma, S. K. Srivastava, *Fiber optic sensors based on plasmonics*, World Scientific, 2015.
- [31] N. A. S. Omar, Y. W. Fen, J. Abdullah, C. E. N. C. E. Chik, M. A. Mahdi, *Sens. Bio-Sensing Res.* **20**, 16 (2018).
- [32] Y. Duan, F. Wang, X. Zhang, Q. Liu, M. Lu, W. Ji, W. Peng, *J. Light. Technol.* **39**(12), 3903 (2021).
- [33] J. Inczédy, T. Lengyel, *Compendium of analytical nomenclature: definitive rules 1997*, Institut d'Estudis Catalans (1998).
- [34] M. S. Soares, M. Vidal, N. F. Santos, F. M. Costa, C. Marques, S. O. Pereira, C. Leitão, *Biosensors* **11**(9), 305 (2021).
- [35] J. Zhong, S. Liu, T. Zou, W. Yan, P. Chen, B. Liu, Z. Sun, Y. Wang, *Sensors* **22**(18), 6824 (2022).
- [36] T. Kumeria, M. M. Rahman, A. Santos, J. Ferre-Borrull, L. F. Marsal, D. Losic, *Anal. Chem.* **86**(3), 1837 (2014).
- [37] Y. C. Chang, J. W. Wu, C. C. Chiang, *Jpn. J. Appl. Phys.* **54**(6S1), 06FP13 (2015).
- [38] D. W. Kim, Y. Zhang, K. L. Cooper, A. Wang, *Appl. Opt.* **44**(26), 5368 (2005).
- [39] S. Y. Cho, N. M. Jokerst, *IEEE Photon. Technol. Lett.* **18**(20), 2096 (2006).
- [40] D. Lu, H. Zhao, X. Zhang, Y. Chen, L. Feng, *Biosensors* **12**(10), 820 (2022).
- [41] J. Huang, Z. Li, Y. Mao, Z. Li, *Nano Select* **2**(8), 1480 (2021).
- [42] R. Kumar, S. Pal, Y. K. Prajapati, J. P. Saini, *Silicon* **13**(6), 1887 (2021).
- [43] X. Wu, Z. Wang, M. Yu, L. Xiu, J. Qiu, *Adv. Mater.* **29**, 1607017 (2017).
- [44] S. Jiang, H. Zhang, Z. Li, L. Chen, L. Yin, X. Liu, *Mater. Today Chem.* **32**, 101638 (2023).

---

\*Corresponding author: harith@um.edu.my